Port-Hamiltonian Macroscopic Modelling based on the Homogenisation Method: case of an acoustic pipe with a porous wall

Alexis Thibault, Thomas Hélie, Henri Boutin, Juliette Chabassier

Port-Hamiltonian Macroscopic Modelling based on the Homogenisation Method: case of an acoustic pipe with a porous wall

Alexis Thibault * **Thomas Hélie** ** **Henri Boutin** **
Juliette Chabassier *

* *Modartt, 9 avenue de l'Europe, Bat. B18, 31520 Ramonville Saint Agne, France (e-mail: thibault@modartt.com, chabassier@modartt.com).*
** *Laboratoire STMS (UMR 9912), IRCAM-CNRS-Sorbonne Université-Ministère de la Culture, 1 place Igor Stravinsky, 75004 Paris, France (e-mail: thomas.helie@ircam.fr, henri.boutin @ircam.fr)*

Abstract: This paper addresses linear propagation in an acoustic pipe with a porous wall, a common scenario in wooden wind instruments. First, a scale separation technique is proposed for dissipative propagation within the wall: the material is modelled as a periodic assembly of identical microscopic cells, forming a network of channels filled with air. It is shown that the resulting PDE admits a port-Hamiltonian formulation, of which the state, flow, effort, Hamiltonian, and differential connection operator are structured using powers of the scale parameter. The resulting macroscopic description, derived from the governing equations at the two lowest orders, manifests as a constrained port-Hamiltonian system involving a Lagrange multiplier. As an example, using an academic cell geometry, we determine the effective wavenumber and dissipation coefficient of a straight tube with a porous wall.

Keywords: Modelling, Homogenisation method, Port-Hamiltonian systems, Distributed parameter systems, Acoustics

1. INTRODUCTION

The propagation of acoustic waves in a wind instrument is slightly influenced by the material used. In the case of wood, the presence of pores (see Figures 1 and 2) can lead to volume dissipation inside the wall. Instrument makers may wish to adjust this effect. In Boutin et al. (2017), the influence of porosity (and surface roughness) was measured on the acoustic input impedance of pipes made from different woods and at different stages (drilling, polishing, oiling) in the instrument manufacturing process. It concluded that oiling reduces acoustic dissipation [1].

To model the effective acoustic behaviour of the porous material without describing each individual pore, Biot (1956a,b) considers a fluid motion in a rigid frame. Assuming that propagation takes place inside a periodic array of rigid-skeleton cells, Allard and Atalla (2009) propose a simpler equivalent fluid model in the frequency domain [2]. Its derivation can be achieved using a scale separation and a homogenisation process to isolate the macroscopic behaviour (see e.g. Allaire and Alouges (2014); Alouges (2016)).

This paper focuses on passive modelling of the macroscopic effect of wall porosity on linear propagation in an acoustic pipe, based on scale separation, the homogenisation method, and its recasting in the port-Hamiltonian framework. As an important result, it reveals that the homogenisation method and the Port-Hamiltonian formulation combine successfully to produce a passive formal structure composed of scale-parameterised objects (state, effort, flow, Hamiltonian, conservative and dissipative connection operators). The truncation of the asymptotic expansion at the two lowest orders provides a description that is used as the macroscopic model [3]. This model defines an interpretable port-Hamiltonian system that involves constraints. It is used to derive the acoustic dispersion relation for the first mode (closest to the plane mode) inside a straight pipe and examine the influence of the porous wall on the wave propagation.

The paper is organised as follows. Section 2 sets the equations of the original linear visco-thermal acoustic problem in a porous wall. Section 3 formulates the problem using scale separation, periodic homogenisation and presents the resulting port-hamiltonian models. Based on the homogenised model, section 4 derives macroscopic loss operators which are involved in acoustics. Finally, numerical solutions are presented for a wall made of cells with an academic geometry, illustrating the resulting effect on the input acoustic impedance of a cylindrical pipe.

[1] This practice is also recommended to musicians for other reasons (see Holder (2018)), such as protecting the wood against variations in temperature and humidity, and the risk of cracking.
[2] See in particular section 5.9 in the article by these authors.
[3] Further mathematical analysis would be required to give mathematical results regarding to the convergence of the double-scale expansion to the homogenised limit, as described by Bensoussan et al. (2011). This study is out of the scope of this paper.

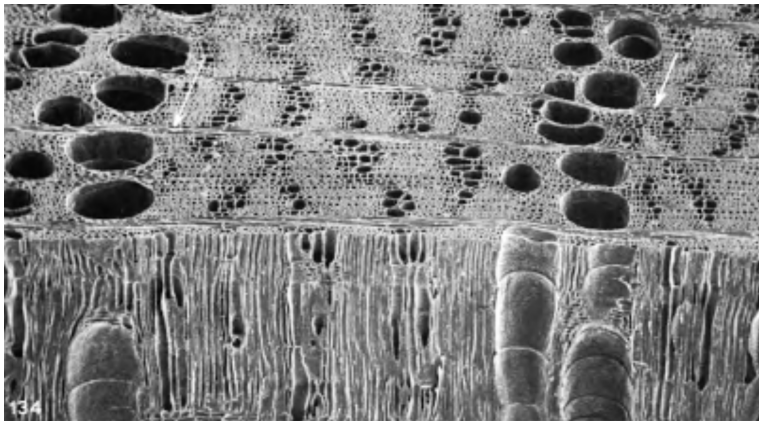

a. (zoom ×80) Transverse (top) and radial longitudinal (bottom) sections of Ulmus procera Salisb. (Fagacaceae)

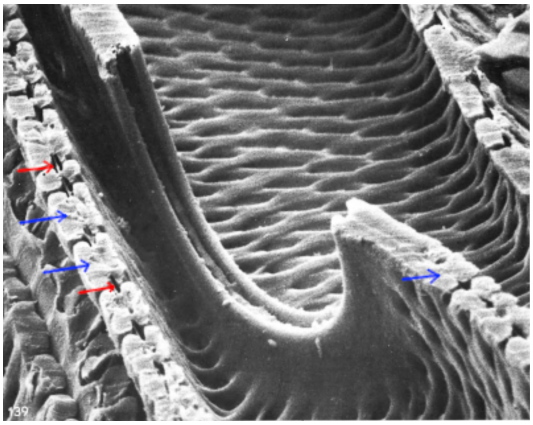

b. (zoom ×3000) Longitudinal radial section of Knightia excelsa R.Br. (Proteaceae)

Fig. 1. Electron microscopy images of wood (extracted from Butterfield et al. (1972)). (a): unevenly distributed vessels on the rings, connected vertically by perforations in their walls (white arrows indicate ring boundaries); (b): simple perforation between two vessel elements, with opening in the secondary wall (red arrows) and closed diaphragms in the primary wall (blue arrows).

2. FLUID EQUATIONS INSIDE THE POROUS WALL

2.1 Hypotheses

Consider the fluid contained inside the bounded connected open set $\Omega_\mathrm{f} \subset \mathbb{R}^d$ of a porous wall and denote $\Gamma_\mathrm{f} \subset \partial\Omega_\mathrm{f}$ the regular boundary between this set and the solid part of the wall. The wood is assumed to be isothermal, at temperature $T_0 \approx 20^o$C. The fluid (air) is characterised at time t and position $\boldsymbol{x}$ by its fields of (total) mass density ρ_tot, particle velocity $\boldsymbol{v}_\mathrm{tot}$, pressure P_tot and temperature T_tot. Air is assumed to behave like a perfect gas, so that $P_\mathrm{tot} = R_0 \rho_\mathrm{tot} T_\mathrm{tot}$ with gas constant $R_0 = 288$ J.kg^{-1}.K^{-1}. Its specific heat capacity at constant pressure is $C_p = \frac{\gamma R_0}{\gamma - 1}$ ≈ 1004 J.kg^{-1}.K^{-1} and heat capacity ratio $\gamma = 1.402$. Its thermal conductivity $\kappa \approx 2.57 \times 10^{-2}$J.m^{-1}.s^{-1}.K^{-1}, shear viscosity $\mu = 1.81 \times 10^{-5}$ kg.m^{-1}.s^{-}1 and bulk viscosity $\zeta = 1.3 \times 10^{-5}$kg.m^{-1}.s^{-1}.

The fluid is assumed to be initially at rest and subjected to small perturbations due to acoustic waves outside the wall. Around the initial homogeneous equilibrium state [4], the field fluctuations $\rho(t,\boldsymbol{x}) = \rho_\mathrm{tot}(t,\boldsymbol{x}) - \rho_0$, $\boldsymbol{v}(t,\boldsymbol{x}) = \boldsymbol{v}_\mathrm{tot}(t,\boldsymbol{x}) - \boldsymbol{0}$, $P(t,\boldsymbol{x}) = P_\mathrm{tot}(t,\boldsymbol{x}) - P_0$ and $T(t,\boldsymbol{x}) = T_\mathrm{tot}(t,\boldsymbol{x}) - T_0$ are then assumed to be small.

2.2 Thermo-visco-acoustic equations

Under these assumptions, the governing equations can be approximated by the linearised Navier-Stokes equations (see e.g. Regev et al. (2016); Bruneau and Potel (2013)):

- Mass conservation in Ω_f
$$\partial_t \rho + \rho_0 \operatorname{div} \boldsymbol{v} = 0, \tag{1a}$$
- Momentum conservation in Ω_f
$$\rho_0 \partial_t \boldsymbol{v} = -\nabla P + \mu \Delta \boldsymbol{v} + \left(\zeta + \frac{\mu}{3}\right) \nabla(\operatorname{div} \boldsymbol{v}), \tag{1b}$$
- Thermal conduction in Ω_f
$$\rho_0 C_p \partial_t T = \kappa \Delta T + \partial_t P, \tag{1c}$$
- Gas state equation in Ω_f
$$P/P_0 = \rho/\rho_0 + T/T_0, \tag{1d}$$
- No-slip condition: $\boldsymbol{v} = 0 \quad$ on Γ_f, (1e)
- Isothermal wall: $T = 0 \quad$ on Γ_f. (1f)

The coupling boundary conditions between the fluid inside and outside the wall are considered in section 4.

2.3 Port-Hamiltonian formulation

Using (1d), equations (1a-1c) rewrite

$$\underbrace{\begin{pmatrix} \frac{1}{P_0} & 0 & -\frac{1}{T_0} \\ 0 & \rho_0 & 0 \\ -\frac{1}{T_0} & 0 & \frac{\rho_0 C_p}{T_0} \end{pmatrix}}_{\mathcal{M}} \underbrace{\begin{pmatrix} \partial_t P \\ \partial_t \boldsymbol{v} \\ \partial_t T \end{pmatrix}}_{\partial_t \boldsymbol{e}} = \underbrace{\begin{pmatrix} 0 & -\operatorname{div} & 0 \\ -\nabla & \mathcal{A} & 0 \\ 0 & 0 & \frac{\kappa}{T_0}\Delta \end{pmatrix}}_{\mathcal{S}} \underbrace{\begin{pmatrix} P \\ \boldsymbol{v} \\ T \end{pmatrix}}_{\boldsymbol{e}}, \tag{2}$$

where $\mathcal{M} = \mathcal{M}^\intercal \succ 0$ is a constant symmetric positive [5] matrix, and the operator $\mathcal{A} = \mu\Delta + \left(\zeta + \frac{\mu}{3}\right)\nabla(\operatorname{div}(\cdot))$ and the Laplacian Δ are negative self-adjoint operators. This describes a linear [6] dissipative port-Hamiltonian system of energy $\frac{1}{2}\langle \boldsymbol{e}, \mathcal{M}\boldsymbol{e}\rangle_{\Omega_\mathrm{f}} = \frac{1}{2}\int_{\Omega_f} \boldsymbol{e}^\intercal \mathcal{M} \boldsymbol{e}\, \mathrm{d}\Omega$, without volume sources, formulated with the co-energy variables $\boldsymbol{e}$ (see Van der Schaft et al. (2014)).

The standard state-space representation is formulated with respect to the energy variable $\boldsymbol{\alpha}$ and the Hamiltonian function H such that $\delta_{\boldsymbol{\alpha}} H = \boldsymbol{e}$, as follows:

$$\partial_t \boldsymbol{\alpha} = \underbrace{(\mathcal{J} - \mathcal{R})}_{\mathcal{S}} \delta_{\boldsymbol{\alpha}} H(\boldsymbol{\alpha}), \tag{3a}$$

$$\text{with } \boldsymbol{\alpha} := \mathcal{M}\,\boldsymbol{e} = \begin{pmatrix} \frac{P}{P_0} - \frac{T}{T_0} = \frac{\rho}{\rho_0} \\ \rho_0 v \\ \rho_0 C_P \frac{T}{T_0} - \frac{P}{T_0} \end{pmatrix} \begin{matrix} \text{relative mass density,} \\ \text{momentum density,} \\ \equiv\text{entropy density,} \end{matrix} \tag{3b}$$

$$H(\boldsymbol{\alpha}) := \frac{1}{2}\langle \mathcal{M}^{-1}\boldsymbol{\alpha}, \boldsymbol{\alpha}\rangle_{\Omega_\mathrm{f}}, \tag{3c}$$

[4] with $\rho_0 = 1.2\,\mathrm{kg.m^{-3}}$, $\boldsymbol{v}_0 = \boldsymbol{0}\,\mathrm{m.s^{-1}}$, $P_0 = 101.3\,\mathrm{Pa}$, $T_0 = 293.15\mathrm{K}$.

[5] Positivity is satisfied since $\rho_0 C_p/(P_0 T_0) = \gamma/(\gamma - 1) > 1$.

[6] See Mora et al. (2021) for a nonlinear formulation.

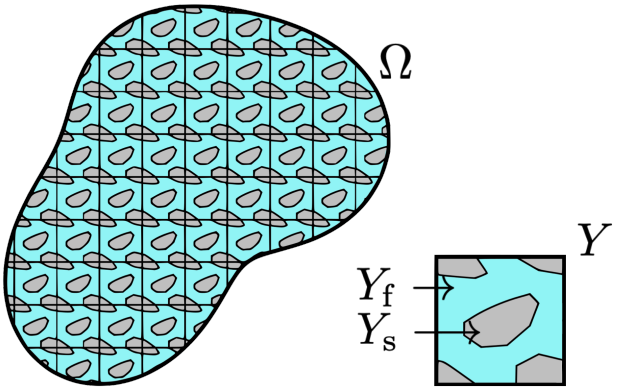

Fig. 2. Schematic of the porous wall domain $\Omega_\varepsilon \subset \Omega$ corresponding to the ε-scale tiling of a representative unit cell of domain Y, occupied by a solid part in Y_s (wood in grey) and a fluid part in Y_f (air in blue).

where $\mathcal{S}$ is decomposed into the skew-symmetric operator

$$\mathcal{J} = -\mathcal{J}^* = \begin{pmatrix} 0 & -\operatorname{div} & 0 \\ -\nabla & 0 & 0 \\ 0 & 0 & 0 \end{pmatrix}, \tag{3d}$$

and a symmetric positive operator

$$\mathcal{R} = \mathcal{R}^* = \begin{pmatrix} 0 & 0 & 0 \\ 0 & -\mathcal{A} & 0 \\ 0 & 0 & \frac{\kappa}{T_0}(-\Delta) \end{pmatrix} \succeq 0. \tag{3e}$$

For null effort $\boldsymbol{e}$ at boundary, the power balance writes $\frac{\mathrm{d}}{\mathrm{d}t} H\big(\boldsymbol{\alpha}(t)\big) = \langle \delta_\alpha H, \dot{\boldsymbol{\alpha}} \rangle_{\Omega_f} = -\langle \delta_\alpha H, -\mathcal{R}\, \delta_\alpha H \rangle_{\Omega_f} \leq 0$.

3. SCALE SEPARATION METHOD: PERIODIC WALL HOMOGENISATION

In order to separate the macroscopic scale at which acoustic propagation takes place (macroscopic length $L_m = 1$ to within one normalisation factor) from the microscopic scale (pore length $L_p \ll L_m$) at which dissipative phenomena take place, a scaling coefficient $\varepsilon = L_p/L_m$ is introduced. The aim of the procedure is to determine the macroscopic behaviour as $\varepsilon \to 0$: this is the "homogenised" effect, in the sense that all the information linked to the ratio of characteristic lengths has been removed.

3.1 Formulation of the homogenisation problem

The wooden porous wall $\Omega \subset (\mathbb{R})^d$ made of solid (Ω_s) and fluid (Ω_f) parts is now assumed to be composed of a periodic array of a representative unit cell.

To distinguish macroscopic and microscopic scales, the microscopic coordinate

$$\boldsymbol{y} = \boldsymbol{x}/\varepsilon \bmod 1, \tag{4}$$

is introduced so that to the macroscopic variable $\boldsymbol{x} \in \Omega$, we associate the corresponding point of the representative microscopic cell Y

$$\boldsymbol{y} \in Y = (\mathbb{R})^d/\mathbb{Z}^d. \tag{5}$$

The cell Y is identified with the unit cube $[0,1]^d$ with periodicity conditions. It is partitioned into a regular, connected, open fluid part Y_f and a solid part Y_s (see figure 2).

The fluid domain Ω_f is now described as the following scale-dependent periodic domain Ω_ε.

Definition 1. The periodic domain Ω_ε is defined as the intersection of Ω with the fluid part of the cell array:

$$\Omega_\varepsilon = \big\{ \boldsymbol{x} \in \Omega \big| \boldsymbol{x}/\varepsilon \in Y_f \big\}. \tag{6}$$

The interfaces with the solid part and with the external environment are respectively $\Gamma_\varepsilon = \big\{ \boldsymbol{x} \in \Omega \big| \boldsymbol{x}/\varepsilon \in \partial Y_f \big\}$ and $\Gamma_\varepsilon^{\text{ext}} = \partial\Omega \cap \partial\Omega_\varepsilon$.

For a scale $\varepsilon > 0$, the fluid movement is governed by (10) in which the fields and the spatial sets are replaced by their scale-dependent counterparts

$$\rho, \boldsymbol{v}, P, T \longrightarrow \rho_\varepsilon, \boldsymbol{v}_\varepsilon, P_\varepsilon, T_\varepsilon, \tag{7a}$$

$$\Omega_f,\, \Gamma_f \longrightarrow \Omega_\varepsilon,\, \Gamma_\varepsilon, \tag{7b}$$

and where the visco-thermal coefficients are made scale-dependent according to the choice of the following ansatz [7]

$$\mu, \eta, \kappa \longrightarrow \varepsilon^2\mu,\, \varepsilon^2\eta,\, \varepsilon^2\kappa, \tag{7c}$$

the physical motivations of which are discussed in (Allard and Atalla, 2009, sec. 5.9).

3.2 Two-scale asymptotic expansion

The double-scale asymptotic expansion technique first consists of assuming that each unknown writes as a power series for the scale parameter ε:

$$\hat{\boldsymbol{v}}_\varepsilon(\boldsymbol{x}) = \hat{\boldsymbol{v}}^{(0)}\big(\boldsymbol{x}, \frac{\boldsymbol{x}}{\varepsilon}\big) + \varepsilon\, \hat{\boldsymbol{v}}^{(1)}\big(\boldsymbol{x}, \frac{\boldsymbol{x}}{\varepsilon}\big) + \varepsilon^2\, \hat{\boldsymbol{v}}^{(2)}\big(\boldsymbol{x}, \frac{\boldsymbol{x}}{\varepsilon}\big) + \dots \tag{8a}$$

$$\hat{P}_\varepsilon(\boldsymbol{x}) = \hat{P}^{(0)}\big(\boldsymbol{x}, \frac{\boldsymbol{x}}{\varepsilon}\big) + \varepsilon\, \hat{P}^{(1)}\big(\boldsymbol{x}, \frac{\boldsymbol{x}}{\varepsilon}\big) + \dots \tag{8b}$$

$$\hat{\rho}'_\varepsilon(\boldsymbol{x}) = \hat{\rho}'^{(0)}\big(\boldsymbol{x}, \frac{\boldsymbol{x}}{\varepsilon}\big) + \varepsilon\, \hat{\rho}'^{(1)}\big(\boldsymbol{x}, \frac{\boldsymbol{x}}{\varepsilon}\big) + \dots \tag{8c}$$

$$\hat{\tau}_\varepsilon(\boldsymbol{x}) = \hat{\tau}^{(0)}\big(\boldsymbol{x}, \frac{\boldsymbol{x}}{\varepsilon}\big) + \varepsilon\, \hat{\tau}^{(1)}\big(\boldsymbol{x}, \frac{\boldsymbol{x}}{\varepsilon}\big) + \dots \tag{8d}$$

where the fields indexed by orders $k = 0, 1, (\dots)$ are functions defined for all $(\boldsymbol{x}, \boldsymbol{y}) \in \Omega \times Y_f$ (meaning that $\boldsymbol{y} \equiv \boldsymbol{x}/\varepsilon$ must be understood "modulo 1").

The second step consists of deriving the first terms of interest (here, $\boldsymbol{v}^{(0)}$ and $P^{(0)}$), which can be interpreted as the homogenised solution, by formally identifying terms of the same degree in ε in the governing equations.

Applying the chain rule to the expressions of the fields (8a-8d), the differentiation operators in space involve different powers of ε. They are expressed as

$$\nabla = \nabla_x + \varepsilon^{-1}\nabla_y, \tag{9a}$$

$$\operatorname{div} = \operatorname{div}_x + \varepsilon^{-1} \operatorname{div}_y, \tag{9b}$$

$$\Delta = \Delta_x + \varepsilon^{-1}(\operatorname{div}_x \nabla_y + \operatorname{div}_y \nabla_x) + \varepsilon^{-2}\Delta_y, \tag{9c}$$

where, for any differential operator D, operators D_x and D_y denote the partial derivative operators with respect to the first and second variable, respectively.

Injecting the power series of the fields into the conservation of mass equation (1a) modified by (7) leads to

$$\partial_t \sum_{k=0}^{\infty} \varepsilon^k \rho^{(k)} + \rho_0 \sum_{k=0}^{\infty} \varepsilon^k \left(\operatorname{div}_x \boldsymbol{v}^{(k)} + \varepsilon^{-1} \operatorname{div}_y \boldsymbol{v}^{(k)} \right) = 0.$$

Similar results are obtained for equations (1b-1f). The formal identification of the terms with homogeneous degree

[7] This artificial manipulation allows the velocity $\boldsymbol{v}_\varepsilon$ to have a non-trivial limit when ε tends to zero, by compensating for shrinking pores by reducing friction.

ε^k leads to a cascade of equations. The degrees ε^{-1} and ε^0 are sufficient to describe the homogenised problem:

- Mass conservation

$$\varepsilon^{-1}: \quad \operatorname{div}_y \boldsymbol{v}^{(0)} = 0, \tag{10a}$$

$$\varepsilon^{0}: \quad \partial_t \rho^{(0)} + \rho_0 \operatorname{div}_x \boldsymbol{v}^{(0)} + \rho_0 \operatorname{div}_y \boldsymbol{v}^{(1)} = 0. \tag{10b}$$

- Momentum conservation

$$\varepsilon^{-1}: \quad \nabla_y P^{(0)} = 0, \tag{10c}$$

$$\varepsilon^{0}: \quad \rho_0 \partial_t \boldsymbol{v}^{(0)} = \mu \Delta_y \boldsymbol{v}^{(0)} + (\zeta + \mu/3)\nabla_y(\operatorname{div}_y \boldsymbol{v}^{(0)}) - \nabla_y P^{(1)} - \nabla_x P^{(0)}. \tag{10d}$$

- Thermal conduction

$$\varepsilon^{0}: \quad \kappa \Delta_y T^{(0)} - \rho_0 C_p \partial_t T^{(0)} = -\partial_t P^{(0)}. \tag{10e}$$

- Gas state equation

$$\varepsilon^{0}: \quad P^{(0)}/P_0 = \rho^{(0)}/\rho_0 + T^{(0)}/T_0. \tag{10f}$$

The boundary conditions stemming from (1e-1f) read [8]

$$\forall (\boldsymbol{x}, \boldsymbol{y}) \in \Omega \times \partial Y_{\mathrm{f}}, \quad \boldsymbol{v}^{(0)}(\boldsymbol{x}, \boldsymbol{y}) = \boldsymbol{v}^{(1)}(\boldsymbol{x}, \boldsymbol{y}) = 0, \tag{11a}$$

$$\forall (\boldsymbol{x}, \boldsymbol{y}) \in \Omega \times \partial Y_{\mathrm{f}}, \quad T^{(0)}(\boldsymbol{x}, \boldsymbol{y}) = 0. \tag{11b}$$

3.3 Port-Hamiltonian formulation

The homogenisation problem described in section 3.1 admits a port-Hamiltonian formulation, which straightforwardly stems from (13a) or (3), by adapting (7a) into

$$\boldsymbol{e},\, \boldsymbol{\alpha} \to \boldsymbol{e}_\varepsilon,\, \boldsymbol{\alpha}_\varepsilon \tag{12}$$

and following the same process as in section 3.2.

n	$\mathcal{J}_n$	$\mathcal{R}_n$
-1	$\begin{pmatrix} 0 & -\operatorname{div}_y & 0 \\ -\nabla_y & 0 & 0 \\ 0 & 0 & 0 \end{pmatrix}$	$0_{3\times 3}$
0	$\begin{pmatrix} 0 & -\operatorname{div}_x & 0 \\ -\nabla_x & 0 & 0 \\ 0 & 0 & 0 \end{pmatrix}$	$\begin{pmatrix} 0 & 0 & 0 \\ 0 & -\mathcal{A}_y & 0 \\ 0 & 0 & -\frac{\kappa}{T_0}\Delta_y \end{pmatrix}$
1	$0_{3\times 3}$	$\begin{pmatrix} 0 & 0 & 0 \\ 0 & -\mathcal{A}_{xy} & 0 \\ 0 & 0 & -\frac{\kappa}{T_0}\Delta_{xy} \end{pmatrix}$
2	$0_{3\times 3}$	$\begin{pmatrix} 0 & 0 & 0 \\ 0 & -\mathcal{A}_x & 0 \\ 0 & 0 & -\frac{\kappa}{T_0}\Delta_x \end{pmatrix}$

Table 1. Decomposition of $\mathcal{S}_\varepsilon = \mathcal{J}_\varepsilon - \mathcal{R}_\varepsilon$ into skew-symmetric and symmetric operators: $\mathcal{J}_\varepsilon = -\mathcal{J}_\varepsilon^\star = \sum_{n=-1}^{0} \varepsilon^n \mathcal{J}_n$ and $\mathcal{R}_\varepsilon = \mathcal{R}_\varepsilon^\star = \sum_{n=0}^{2} \varepsilon^n \mathcal{R}_n \succeq 0$. Operators $\mathcal{J}_n$ and $\mathcal{R}_n$ with their dependence on x or y detail how the conservative and dissipative phenomena are fed and structured by the macroscopic (x) or microscopic (y) scales for each scale-degree transfer n. Note that the homogeneised problem (16) only involves $n = -1$ and 0.

Co-energy variables. The port-Hamiltonian formulation written for the co-energy variables $\boldsymbol{e}_\varepsilon = [p_\varepsilon, \boldsymbol{v}_\varepsilon^\intercal, T_\varepsilon]^\intercal$ is

$$\mathcal{M}\, \partial_t \boldsymbol{e}_\varepsilon = \mathcal{S}_\varepsilon \boldsymbol{e}_\varepsilon, \tag{13a}$$

where operator $\mathcal{S}_\varepsilon$ is formally negative and given by

$$\mathcal{S}_\varepsilon = \varepsilon^{-1}\mathcal{S}_{-1} + \mathcal{S}_0 + \varepsilon \mathcal{S}_1 + \varepsilon^2 \mathcal{S}_2, \tag{13b}$$

[8] For more details, see the PhD manuscript (Thibault, 2023, p. 169).

with (see also table 1 for a detailed decomposition)

$$\mathcal{S}_{-1} = \begin{pmatrix} 0 & -\operatorname{div}_y & 0 \\ -\nabla_y & 0 & 0 \\ 0 & 0 & 0 \end{pmatrix} \quad \mathcal{S}_0 = \begin{pmatrix} 0 & -\operatorname{div}_x & 0 \\ -\nabla_x & \mathcal{A}_y & 0 \\ 0 & 0 & \frac{\kappa}{T_0}\Delta_y \end{pmatrix}$$

$$\mathcal{S}_1 = \begin{pmatrix} 0 & 0 & 0 \\ 0 & \mathcal{A}_{xy} & 0 \\ 0 & 0 & \frac{\kappa}{T_0}\Delta_{xy} \end{pmatrix} \quad \mathcal{S}_2 = \begin{pmatrix} 0 & 0 & 0 \\ 0 & \mathcal{A}_x & 0 \\ 0 & 0 & \frac{\kappa}{T_0}\Delta_x \end{pmatrix}, \tag{13c}$$

and where the differential operators are defined by

$$\Delta_{xy} = \operatorname{div}_x \nabla_y + \operatorname{div}_y \nabla x, \tag{13d}$$

$$\mathcal{A}_y = \mu \Delta_y + \left(\zeta + \frac{\mu}{3}\right) \nabla_y(\operatorname{div}_y(\cdot)), \tag{13e}$$

$$\mathcal{A}_{xy} = \mu \Delta_{xy} + \left(\zeta + \frac{\mu}{3}\right) \left(\nabla_x(\operatorname{div}_y(\cdot)) + \nabla_y(\operatorname{div}_x(\cdot))\right), \tag{13f}$$

$$\mathcal{A}_x = \mu \Delta_x + \left(\zeta + \frac{\mu}{3}\right) \nabla_x(\operatorname{div}_x(\cdot)). \tag{13g}$$

The energy of the system

$$\mathcal{E}_\varepsilon(t) = \frac{1}{2}\left\langle \boldsymbol{x} \mapsto e_\varepsilon(t, \boldsymbol{x}, \boldsymbol{x}/\varepsilon)\,,\, \boldsymbol{x} \mapsto \mathcal{M}\, e_\varepsilon(t, \boldsymbol{x}, \boldsymbol{x}/\varepsilon) \right\rangle_{\Omega_\varepsilon}$$
$$= \frac{1}{2}\int_{\Omega_\varepsilon} \sum_{k_1, k_2 \geq 0} \varepsilon^{k_1+k_2} \boldsymbol{e}^{(k_1)}\big(t, \boldsymbol{x}, \frac{\boldsymbol{x}}{\varepsilon}\big)^\intercal \mathcal{M} \boldsymbol{e}^{(k_2)}\big(t, \boldsymbol{x}, \frac{\boldsymbol{x}}{\varepsilon}\big)\, \mathrm{d}\Omega$$

is also structured by the scale parameter ε.

The evolution equation (13a) rewrites

$$\mathcal{M} \sum_{k=0}^{\infty} \varepsilon^k \partial_t \boldsymbol{e}^{(k)} = \sum_{n=-1}^{2} \varepsilon^n \mathcal{S}_n \sum_{k=0}^{\infty} \varepsilon^k \boldsymbol{e}^{(k)}. \tag{14}$$

Identifying terms of the same degree in ε yields

$$\varepsilon^{-1}: \quad 0 = \mathcal{S}_{-1}\boldsymbol{e}^{(0)}, \tag{15a}$$

$$\varepsilon^{0}: \quad \mathcal{M}\partial_t \boldsymbol{e}^{(0)} = \mathcal{S}_{-1}\boldsymbol{e}^{(1)} + \mathcal{S}_0 \boldsymbol{e}^{(0)}, \tag{15b}$$

$$\varepsilon^{1}: \quad \mathcal{M}\partial_t \boldsymbol{e}^{(1)} t = \mathcal{S}_{-1}\boldsymbol{e}^{(2)} + \mathcal{S}_0 \boldsymbol{e}^{(1)} + \mathcal{S}_1 \boldsymbol{e}^{(0)}, \tag{15c}$$

$$\varepsilon^{k}, k \geq 2: \quad \mathcal{M}\partial_t \boldsymbol{e}^{(k)} = \mathcal{S}_{-1}\boldsymbol{e}^{(k+1)} + \mathcal{S}_0 \boldsymbol{e}^{(k)} + \mathcal{S}_1 \boldsymbol{e}^{(k-1)} + \mathcal{S}_2 \boldsymbol{e}^{(k-2)}. \tag{15d}$$

The system of equations (10) considered above corresponds to (15a-15b). Note that this pair of equations, which defines the homogenised problem, is also a port-Hamiltonian system:

$$\begin{pmatrix} \mathcal{M}\partial_t \boldsymbol{e}^{(0)} \\ 0 \end{pmatrix} = \begin{pmatrix} \mathcal{S}_0 & \mathcal{S}_{-1} \\ \mathcal{S}_{-1} & 0 \end{pmatrix} \begin{pmatrix} \boldsymbol{e}^{(0)} \\ \boldsymbol{e}^{(1)} \end{pmatrix}, \tag{16}$$

where the operator in the right-hand side is formally negative, because $\mathcal{S}_0$ is negative and $\mathcal{S}_{-1}$ is formally skew-adjoint (see table 1). As in section 3.2, the unknown $\boldsymbol{e}^{(1)}$ serves as the Lagrange multiplier associated with the constraint.

Energy variables. Following the same process for (3-3e), the state-space representation with respect to the energy variable $\boldsymbol{\alpha}_\varepsilon$ is

$$\underbrace{\partial_t \boldsymbol{\alpha}_\varepsilon}_{\mathcal{M}\partial_t \boldsymbol{e}_\varepsilon} = \underbrace{(\mathcal{J}_\varepsilon - \mathcal{R}_\varepsilon)}_{\mathcal{S}_\varepsilon} \underbrace{\delta_{\boldsymbol{\alpha}_\varepsilon} H_\varepsilon(\boldsymbol{\alpha}_\varepsilon)}_{\mathcal{M}^{-1}\boldsymbol{\alpha}_\varepsilon = \boldsymbol{e}_\varepsilon}, \tag{17a}$$

$$\text{with } \boldsymbol{\alpha}_\varepsilon := \mathcal{M}\, \boldsymbol{e}_\varepsilon \tag{17b}$$

$$\text{and } H_\varepsilon(\boldsymbol{\alpha}_\varepsilon) := \frac{1}{2}\langle \mathcal{M}^{-1}\boldsymbol{\alpha}_\varepsilon, \boldsymbol{\alpha}_\varepsilon \rangle_{\Omega_\varepsilon}, \tag{17c}$$

The port-Hamiltonian system of the homogenised problem (equivalent to (16)) is

$$\begin{pmatrix} \partial_t \boldsymbol{\alpha}^{(0)} \\ 0 \end{pmatrix} = \begin{pmatrix} \mathcal{S}_0 & \mathcal{S}_{-1} \\ \mathcal{S}_{-1} & 0 \end{pmatrix} \begin{pmatrix} \mathcal{M}^{-1}\boldsymbol{\alpha}^{(0)} \\ \mathcal{M}^{-1}\boldsymbol{\alpha}^{(1)} \end{pmatrix}. \tag{18}$$

4. MACROSCOPIC LOSS OPERATORS IN THE LAPLACE DOMAIN AND APPLICATION

The homogenised problem describes the macroscopic dissipation due to the thermo-viscous phenomena involved at microscopic scale in a porous media. This section briefly introduces some related loss operators in the spectral domain, and gives an illustration of their effect on a cylindrical acoustic pipe with a porous wall for an academic cell geometry (see Thibault (2023) for a detailed presentation).

To this end, the linear problem (10-11) is addressed in the spectral domain. In the following, we consider the Laplace variable $s \in \overline{\mathbb{C}_0^+} = \{s \in \mathbb{C} \,|\, \mathrm{Re}(s) \geq 0\}$ (or $s = \mathrm{i}\omega \in \mathrm{i}\mathbb{R}$ for the Fourier domain). The fields expressed in the spectral domain are denoted with a hat symbol.

4.1 Fields $\hat{P}^{(0)}$, $\hat{T}^{(0)}$ and $\hat{\boldsymbol{v}}^{(0)}$

In this subsection, variable s is omitted for conciseness. From (10c), the first pressure term $\hat{P}^{(0)}$ depends only on $\boldsymbol{x}$ (in other words, it appears constant at microscopic scale). After calculations, it can be shown that fields $\hat{T}^{(0)}$ and $\hat{\boldsymbol{v}}^{(0)}$ are related to $\hat{P}^{(0)}$ as

$$\hat{\tau}^{(0)}(\boldsymbol{x},\boldsymbol{y}) = \hat{P}^{(0)}(\boldsymbol{x})\,\varphi(\boldsymbol{y}), \tag{19}$$

$$\hat{\boldsymbol{v}}^{(0)}(\boldsymbol{x},\boldsymbol{y}) = \sum_{i=1}^{d} \boldsymbol{w}_i(\boldsymbol{y}) \frac{\partial \hat{\hat{P}}^{(0)}}{\partial x_i}(\boldsymbol{x}), \tag{20}$$

where φ and $(\boldsymbol{w}_i, q_i)$ are solutions to boundary problems in the unit cell ($\boldsymbol{E}_i$ denotes the unit vector oriented in direction i):

$$\begin{cases} \kappa\,\Delta\varphi(\boldsymbol{y}) - s\rho_0 C_p\,\varphi(\boldsymbol{y}) = -s \;\text{ on } Y_\mathrm{f}, \\ \varphi|_{\partial Y_\mathrm{f}} = 0, \end{cases} \tag{21}$$

$$\begin{cases} \mu\Delta\boldsymbol{w}_i(\boldsymbol{y}) - \nabla q_i(\boldsymbol{y}) - s\rho_0\,\boldsymbol{w}_i(\boldsymbol{y}) = \boldsymbol{E}_i \;\text{ on } Y_\mathrm{f} \\ \mathrm{div}\,\boldsymbol{w}_i(\boldsymbol{y}) = 0 \;\text{ on } Y_\mathrm{f} \\ \boldsymbol{w}_i|_{\partial Y_\mathrm{f}} = 0. \end{cases} \tag{22}$$

4.2 Effective fluid and loss coefficients in acoustic pipes

It is shown (see (Thibault, 2023, Eq. (6.32) and remark 6.5)) that:

- these fields corresponds to an effective fluid characterised by

$$\rho_e(s) = -\frac{1}{s}\,\hat{\boldsymbol{A}}^{-1}(s), \qquad \text{(density)} \tag{23a}$$

$$K_e(s) = \frac{1}{1/P_0 - \hat{B}(s)/T_0}, \qquad \text{(compressibility)} \tag{23b}$$

- the loss coefficients (analog to those involved in acoustic pipes with boundary layers) that represent the macroscopic dissipation inside the porous wall are

$$K_t(s) = 1 - \rho_0 C_p \hat{B}(s), \qquad \text{(thermal)} \tag{24a}$$

$$\boldsymbol{K}_v(s) = \boldsymbol{I}_d + \rho_0 s\hat{\boldsymbol{A}}(s), \qquad \text{(viscous)} \tag{24b}$$

where the permeability operators are defined by $\hat{\boldsymbol{A}}\boldsymbol{E}_i = \langle \boldsymbol{w}_i \rangle$ and $\hat{B} = \langle \varphi \rangle$ with the average operator $\langle \cdot \rangle = \int_{Y_f} \cdot\,\mathrm{d}\boldsymbol{y} / \int_{Y_f} 1\,\mathrm{d}\boldsymbol{y}$.

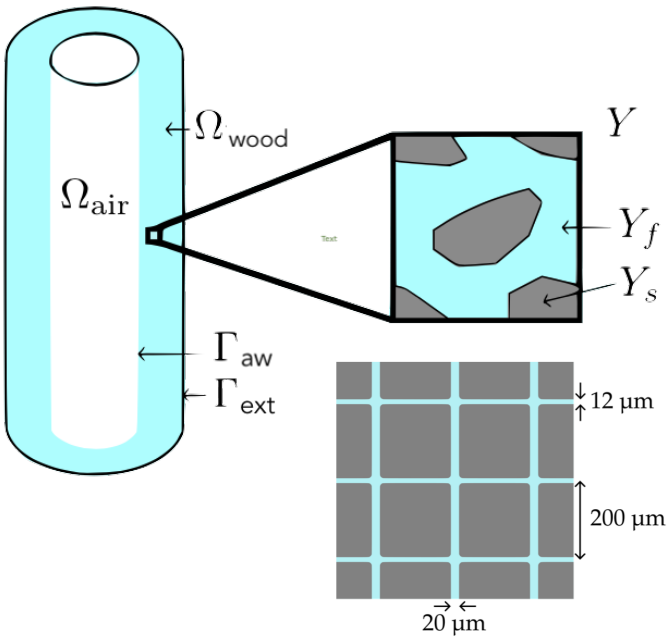

Fig. 3. Cylindrical pipe with a porous wall (top) and example of a 2D academic cell (bottom).

4.3 Wave equation in an acoustic pipe with a porous wall

Consider a cylindrical pipe with a porous wall, a circular base and an internal radius R and an external radius R_{ext} (see figure 3).

Waves propagate without attenuation inside the pipe filled with air (Ω_{air}) and are attentuated inside the porous wall Ω_{wood}. The interface between the two media is denoted Γ_{ab} and the outer wall Γ_{ext}. These sets are described in cylindrical coordinates $\boldsymbol{x} = (r, \theta, z)$ by

$$\Omega_{\text{air}} = \{\boldsymbol{x} \mid r < R\}, \quad \Omega_{\text{wood}} = \{\boldsymbol{x} \mid R < r < R_{\text{ext}}\},$$
$$\Gamma_{\text{ab}} = \{\boldsymbol{x} \mid r = R\}, \quad \Gamma_{\text{ext}} = \{\boldsymbol{x} \mid r = R_{\text{ext}}\}.$$

Studying the acoustic coupling between Ω_{air} and Ω_{wood}, it is shown that the wave propagation in $\Omega_{\text{air}} \cup \Omega_{\text{wood}}$ is governed by

$$\widetilde{\rho}_e(s,\boldsymbol{x})\,s\,\widetilde{\boldsymbol{v}}(s,\boldsymbol{x}) = -\nabla\hat{P}^{(0)}(s,\boldsymbol{x}) \tag{25a}$$

$$s\,\hat{P}^{(0)}(s,\boldsymbol{x}) = -\widetilde{K}_e(s,\boldsymbol{x})\,\mathrm{div}\,\widetilde{\boldsymbol{v}}(s,\boldsymbol{x}) \tag{25b}$$

where $\widetilde{\boldsymbol{v}} = \hat{\boldsymbol{v}}$, $\widetilde{K}_e = \gamma P_0$, $\widetilde{\rho}_e = \rho_0$ in Ω_{air}, and where $\widetilde{\boldsymbol{v}}(s,\boldsymbol{x}) = \phi\,\langle\hat{\boldsymbol{v}}\rangle(s,\boldsymbol{x})$, $\widetilde{K}_e(s,\boldsymbol{x}) = \frac{K_e(s)}{\phi}$, $\widetilde{\rho}_e(s,\boldsymbol{x}) = \frac{\rho_e(s)}{\phi}$ for $\boldsymbol{x} \in \Omega_{\text{bois}}$. In these formula, $\phi := |Y_\mathrm{f}|/|Y|$ denotes the porosity coefficient, ρ_e and K_e are defined in (23), K_t and $\boldsymbol{K}_v$ are defined in (24).

Eliminating $\tilde{v}$ in (25) leads to a Helmholtz equation (in the Laplace domain, or choosing $s = \mathrm{i}\omega$)

$$s^2\,\widetilde{K}_e^{-1}(s,\boldsymbol{x})\,\hat{P}^{(0)}(s,\boldsymbol{x}) - \mathrm{div}\big(\widetilde{\rho}_e^{-1}(s,\boldsymbol{x})\,\nabla\hat{P}^{(0)}(s,\boldsymbol{x})\big) = 0. \tag{26}$$

We assume that the amount of energy leaking outside the instrument is negligible, so that we can avoid modelling what happens around the pipe. In this case, the boundary condition is

$$\hat{P}^{(0)} = 0 \quad \text{on } \Gamma_{\text{ext}}. \tag{27}$$

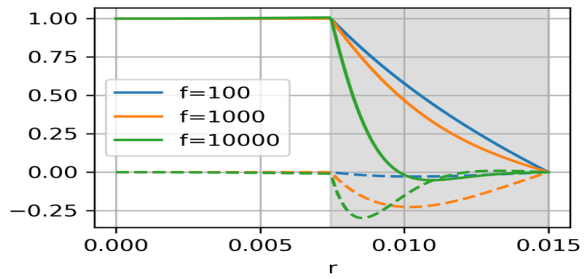

Fig. 4. Radial profile of the first pressure mode at different frequencies f: real (-) and imaginary(--) parts; grey background Ω_{wood}. The vertical scale is arbitrary.

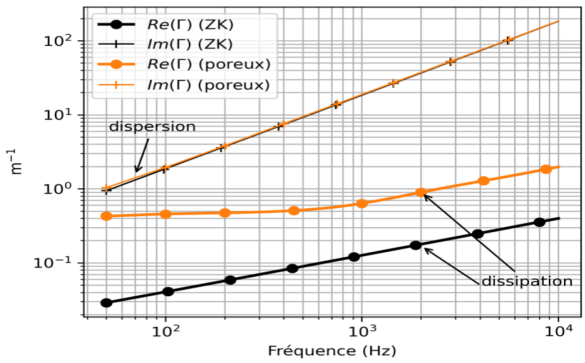

Fig. 5. Complex wavenumber: (black) perfect wall (Zwicker-Kosten model); orange: porous wall (academic geometry with exaggerated porosity).

4.4 Numerical results

Simulations have been processed for a pipe with parameters $R = 7.45\,\text{mm}$, $R_{\text{ext}} = 15.0\,\text{mm}$ and porosity $\phi = 0.156$ that corresponds to a cell with the academic geometry pictured in figure 3 (bottom part). The steps are (Thibault, 2023, sections 6.5-6.6): solve the cell problem using the high-order finite element code *Montjoie* (see Duruflé (2021)); derive the dispersion relationship of the first pressure mode (closest to the planar mode). Figures 4, 5 and 6 respectively present the resulting radial profile, wavenumber and input impedance for the length $L = 240.5\,\text{mm}$.

5. CONCLUSION

This article shows the interest of combining the homogenisation method and the port-Hamiltonian formulation: this enables the passivity of microscopic phenomena to be characterised at several scales and this produces passive macroscopic descriptions.

A perspective is concerned with the convergence analysis of the solutions. Moreover, it would be interesting to examine this approach on nonlinear systems.

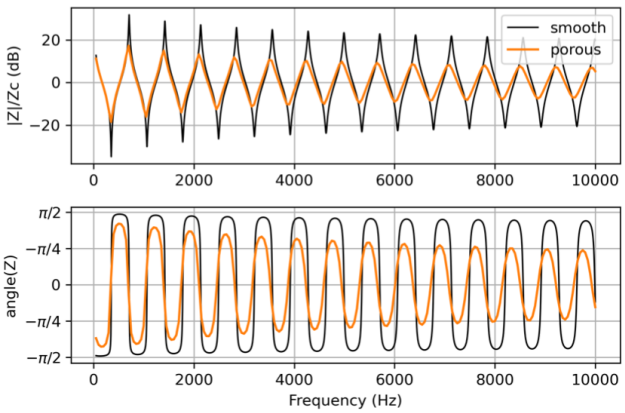

Fig. 6. Normalised input impedance of a pipe: (black) perfect wall (Zwikker-Kosten model); (orange) porous wall (academic geometry with exaggerated porosity).

REFERENCES

Allaire, G. and Alouges, F. (2014). Introduction to homogenization theory. http://www.cmap.polytechnique.fr/∼allaire/homogenization.html.

Allard, J.F. and Atalla, N. (2009). *Propagation of sound in porous media: modelling sound absorbing materials*. John Wiley & Sons, 2nd edition.

Alouges, F. (2016). Introduction to periodic homogenization. *Interdiscipl. Information Sciences*, 22(2), 147–186.

Bensoussan, A., Lions, J.L., and Papanicolaou, G. (2011). *Asymptotic analysis for periodic structures*, volume 374. American Mathematical Soc.

Biot, M.A. (1956a). Theory of propagation of elastic waves in a fluid-saturated porous solid. I. low-frequency range. *J. Acoust. Soc. of America*, 28(2), 168–178.

Biot, M.A. (1956b). Theory of propagation of elastic waves in a fluid-saturated porous solid. II. Higher frequency range. *J. Acoust. Soc. of America*, 28(2), 179–191.

Boutin, H., Le Conte, S., Vaiedelich, S., Fabre, B., and Le Carrou, J.L. (2017). Acoustic dissipation in wooden pipes of different species used in wind instrument making: An experimental study. *J. Acoust. Soc. of America*, 141(4), 2840–2848.

Bruneau, M. and Potel, C. (2013). *Materials and acoustics handbook*. John Wiley & Sons.

Butterfield, B., Meylan, B., et al. (1972). *Three-dimensional structure of wood: An Ultrastructural Approach*. Dordrecht: Springer Netherlands.

Duruflé, M. (2021). Montjoie software. https://www.math.u-bordeaux.fr/∼durufle/montjoie/.

Holder, A. (2018). *Clarinet Repair and Maintenance: Perspectives on Basic Repair Topics for Performers*. Ph.D. thesis, The Florida State University.

Mora, L.A., Le Gorrec, Y., Matignon, D., Ramirez, H., and Yuz, J.I. (2021). On port-Hamiltonian formulations of 3-dimensional compressible Newtonian fluids. *Physics of Fluids*, 33(11).

Regev, O., Umurhan, O.M., and Yecko, P.A. (2016). *Modern fluid dynamics for physics and astrophysics*. Springer Science & Business Media.

Thibault, A. (2023). *Modélisation, analyse et simulation de l'acoustique dissipative dans les tubes poreux ou rugueux - Application aux instruments à vent*. Phd thesis, Université de Pau et des Pays de l'Adour.

Van der Schaft, A., Jeltsema, D., et al. (2014). Port-hamiltonian systems theory: An introductory overview. *Foundations and Trends® in Systems and Control*, 1(2-3), 173–378.